Ocean Engineering 266 (2022) 113024

Contents lists available at ScienceDirect

Ocean Engineering

journal homepage: www.elsevier.com/locate/oceaneng

Experimental flow control investigation over suction surface of turbine blade with local surface passive oscillation

Kemal Koca [a,b], Mustafa Serdar Genç [a,c,d,*], Dhamotharan Veerasamy [e], Mustafa Özden [a,f]

[a] Wind Engineering and Aerodynamic Research Center, Department of Energy Systems Engineering, Erciyes University, 38039, Kayseri, Turkey
[b] Department of Mechanical Engineering, Abdullah Gül University, 38080, Kayseri, Turkey
[c] Energy Conversion Research and Application Center, Erciyes University, 38039, Kayseri, Turkey
[d] MSG Teknoloji Ltd. Şti, Erciyes Teknopark Tekno-1 Binası, 61/20, 38039, Kayseri, Turkey
[e] School of Engineering, Newcastle University, Newcastle Upon Tyne, NE1 7RU, United Kingdom
[f] Scientific Research Projects Unit of Erciyes University, Erciyes University, 38039, Kayseri, Turkey

ARTICLE INFO

Keywords:
Local flexible membrane
Passive flow control
Intermittency
Laminar separation bubble
Suction surface of Clark-Y airfoil

ABSTRACT

Impact of the local flexible membrane (LFM) on aerodynamic phenomena including the formation of a laminar separation bubble (LSB) and transition to turbulence was experimentally investigated over the suction surface of a Clark-Y airfoil first time in literature. The experiments such as aerodynamic force measurement, smoke-wire flow visualization and hot-film tests were carried out at the free-stream velocity of $U_\infty = 3.2$ m/s, $U_\infty = 6.4$ m/s, $U_\infty = 9.6$ m/s, $U_\infty = 12.8$ m/s, and Reynolds number based upon on the chord length was $Re_c = 3.5 \times 10^4$, $Re_c = 7.0 \times 10^4$, $Re_c = 1.05 \times 10^5$ and $Re_c = 1.4 \times 10^5$, respectively. The experimental angle of attack was set at $0^\circ = \alpha \leq 20^\circ$. In detailed intermittency analysis by the hot-film sensor over the uncontrolled airfoil, it was seen that the LSB and transition to turbulence formed close to the trailing edge at a lower angle of attack, and it moved towards the leading edge when increasing the angle of attack simultaneously. Employing LFM on the suction surface obviously affected the progress of these flow phenomena. In the results of smoke-wire flow visualization, either the size of the laminar separation bubble (LSB) was reduced or its presence was suppressed at lower incidences. The aerodynamic force measurement results also supported those behaviors. In particular, at lower incidences, the negative effects of LSB were mitigated, resulting in the presence of a more stable lift curve. Additionally, it was clearly observed that utilizing LFM ensured positive effects, especially at the pre- and the post-stall regions in terms of fewer fluctuations at the C_L curve, meaning that less aerodynamic vibration and noise on wind/hydro turbine could be obtained.

1. Introduction

Growing interest in wind/hydropower and unmanned air vehicles has been pushed and rekindled by researchers who are keen on investigating flow regimes at low Reynolds numbers. Turbine blades typically operated at Reynolds numbers of 10^4-10^5, which developed complex aerodynamic properties including unsteady flow characteristics over the suction surface of airfoils. The flow cannot cope with the effects of severe adverse pressure gradients (APGs) in the aforementioned flow regimes, and it enters the tendency of separating from the solid surface at the laminar regime, resulting in presence of a separated shear layer. This shear layer separated from the surface at larger angles of attack (AoA), causing the stall condition. This leads to global alteration in the pressure distribution for both surfaces. Major deterioration of airfoil performance is inevitable in these conditions. Furthermore, the transition phenomenon in the separated flow can be formed due to the presence of strong amplifications of disturbances at moderate AoA but still below Reynolds number of 5×10^5. After a while, the motion of turbulent fluctuations boosts in the vertical direction to flow and triggers an aerodynamic deflection of separated flow to the solid surface of airfoil. This energized flow eventually causes the separated layer to tread the solid surface. The area among reattachment and separation points was commonly named as laminar separation bubble (LSB) in the literature.

In terms of a better determination of LSB, it was sketched on the upper surface of Clark-Y airfoil as illustrated in Fig. 1. At a low Reynolds number, the boundary layer on the airfoil is laminar but the velocity

* Corresponding author. Wind Engineering and Aerodynamic Research Laboratory, Department of Energy Systems Engineering, Erciyes University, 38039, Kayseri, Turkey.
E-mail address: musgenc@erciyes.edu.tr (M.S. Genç).

https://doi.org/10.1016/j.oceaneng.2022.113024
Received 9 August 2022; Received in revised form 13 October 2022; Accepted 26 October 2022
Available online 5 November 2022

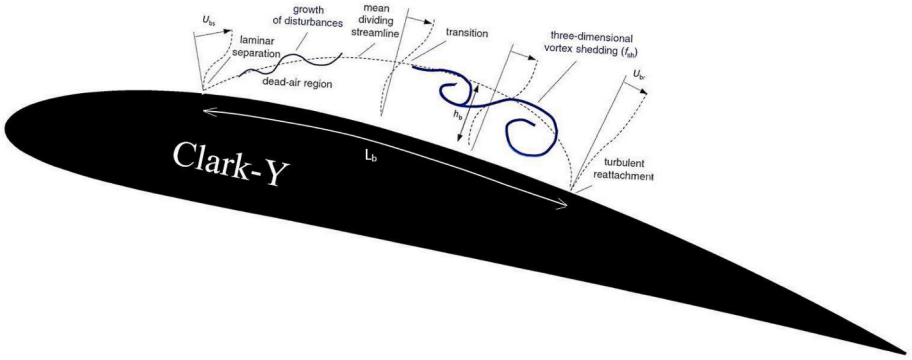

Fig. 1. Simplified schematic of LSB formation on the suction surface of Clark-Y airfoil (not to scaled).

Table 1
Technical specifications of the wind tunnel.

Design	Suction type and low speed
Length of tunnel	13 m
Test section	Length (4 m), Height (0.5 m), Width (0.5 m)
Motor	Type: DC motor, Power: 15 kW, Frequency: 50 Hz
Model	H4, 1000/15A
Capacity	45000 m^3/h, 450 PA
Flow velocity	5 m/s < U < 40 m/s
Turbulence level	0.3% < Tu < ~0.9%
Nozzle	Contraction cone: 9:1

potential is unstable. The laminar flow encounters the APGs and it separates from the solid surface. As mentioned, in the previous study by current authors (Koca et al., 2021), $\frac{du}{dy}$ is zero in the separation point. Then, the hydrodynamic instability such as the presence of Tollmien-Schlichting (T-S) wave is able to transfer downstream by means of convection. The disturbances grow until the transition occurs on a solid surface. The pressure distribution is comparatively zero between the laminar separation and transition onset which $\frac{du}{dy}$ is less than zero. Hence, that region is called a dead air region (Genç et al., 2008, 2016a; Açıkel and Genç, 2016; Koca et al., 2022a). After the transition, three-dimensional vortex sheds and turbulence spots are observed until the presence of turbulent reattachment.

As one of the pioneering studies performed by Gaster (1966), the presence of LSB as well as transition to turbulence phenomenon may negatively affect the airfoil performance due to the local change of surface pressure distribution. A reliable and robust method to predict the transition onset and location of LSB was deemed very crucial for the blade/wing designs. Hence, the detection of the presence of LSB, transition to turbulence, and boundary layer separation over wind turbine airfoils is of particular interest.

The presence of LSB and prediction of transition onset have been investigated numerically and experimentally so far. As an aspect of the numerical study, a Reynolds Averaged Navier Stokes (RANS) solver was employed by Yuan et al. (2005) and Windte (Windte et al., 2006) to predict the transition. They highlighted the contour plots of Reynolds stresses in their study. Genç et al. (2011) employed the k-k_L-ω transition model for the prediction of LSB formation on NACA 2415 airfoil by conducting with/without blowing and suction at Reynolds number of 2 × 10^5 and α = 8°. Their results consisted twofold: (*i*) firstly, the results obtained by the transition model exhibited well coherence with prior hot-wire measurements, and (*ii*) secondly, it was observed that LSB formation was suppressed by utilizing suction and blowing simultaneously, resulting in aerodynamic lift increment and drag loss. A

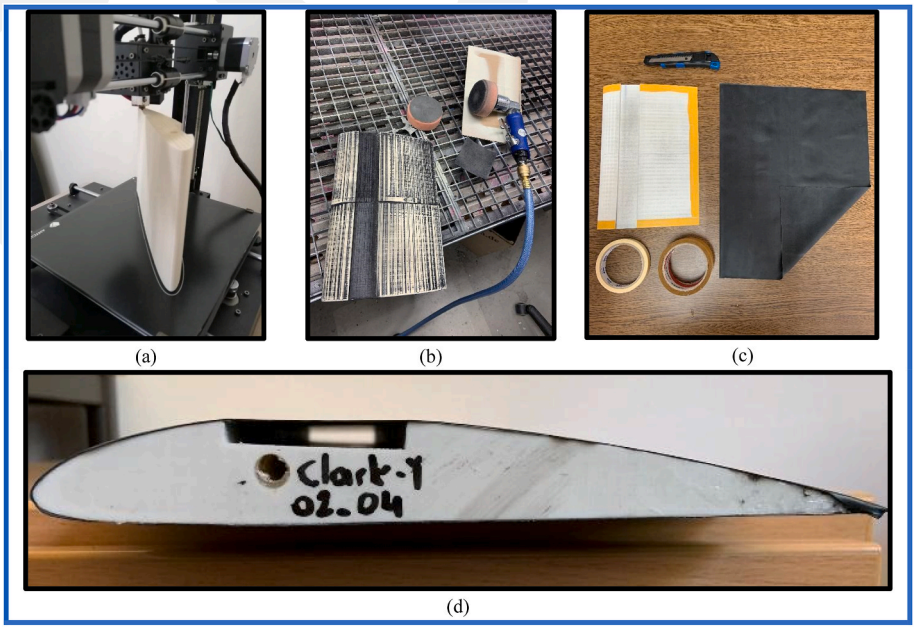

Fig. 2. The layouts of the controlled Clark-Y airfoil with LFM, a) manufacturing process of the airfoil, b) surface cleaning process, c) covering all surfaces of the airfoil with latex rubber sheet, d) closed view of Clark-Y airfoil with LFM.

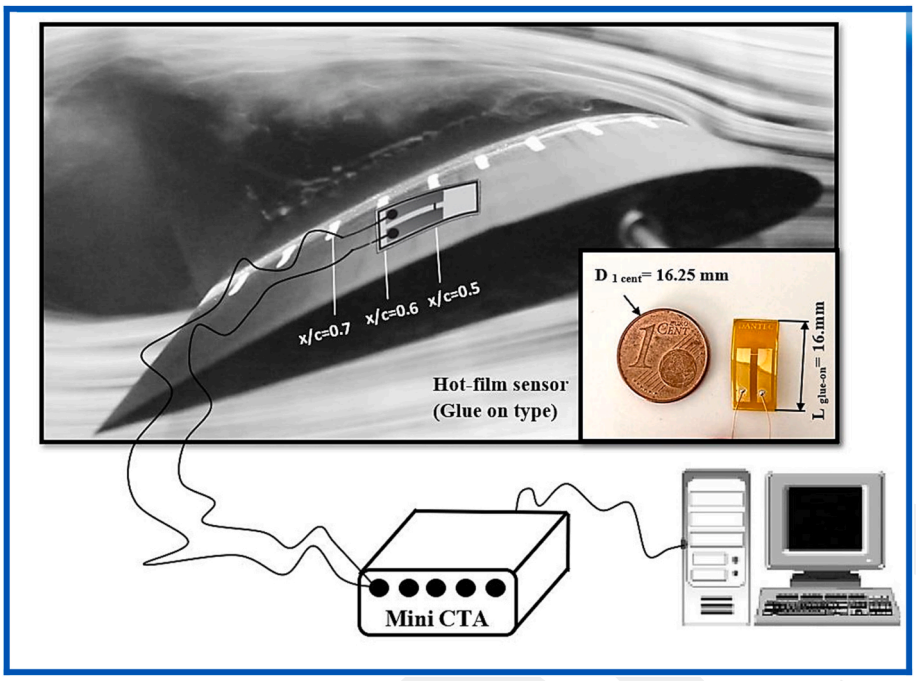

Fig. 3. Locations of hot-film sensor throughout chordwise over suction surface.

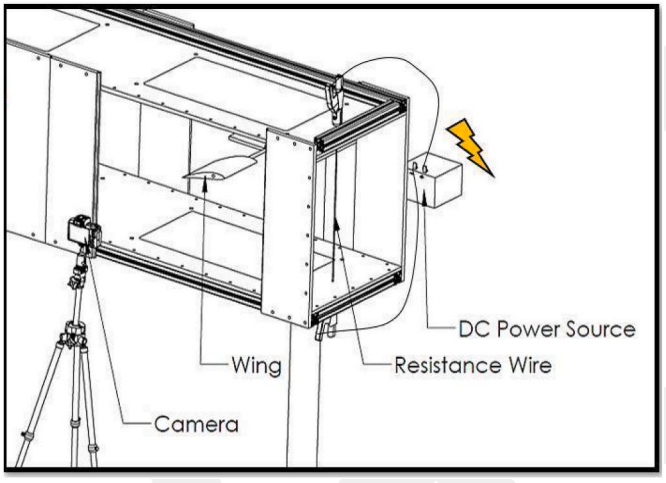

Fig. 4. The sketch of smoke-wire test apparatus.

high-order implicit Large Eddy Simulation (LES) was applied by Galbraith and Visbal (2008) to investigate the drag polar over SD7003 airfoil at Reynolds number of 6×10^4. Their results included that good accuracy was captured in conjunction with the data obtained from experiments. The stall was well predicted. At the post-stall angle, the result of C_L exhibited well coherence with the experiments, whereas the results of C_D were over-predicted. Karasu et al. (2018) investigated the performance assessment of transition models including k-k_L-ω and k-ω SST (Shear Stress Transport) on NACA 4412 airfoil having aspect ratios (AR) of 1, 3 at various Reynolds numbers and angles of attack. The results acquired by numerical simulation were compared with the experimental results (Genç et al., 2018), and it was concluded that the LSB formation and tip vortices were successfully predicted except for a few discrepancies of C_L. Transition to turbulence was captured at low Reynolds flows in conjunction with good accuracy by utilizing Direct Numerical Simulation (DNS) in the studies performed by Durbin et al. (Durbin, 2002) and Zheng et al. (1998).

Apart from numerical studies, experimental investigations were frequently performed by the researchers in terms of prediction of transition onset and progress of LSB even though they had time-consuming preparation and a high level of instrumentation. These techniques consisted of utilizing Particle Image Velocimetry (PIV) (Hain et al., 2009; Wolf et al., 2011; Jagadeesh et al., 2013; Bhattacharya and Ahmed, 2020; Bhattacharya and Gregory, 2018, 2020), surface oil film visualization (Genç et al., 2018; Schülein, 2004), pressure distribution (Genç et al., 2012; Istvan and Yarusevych, 2018), smoke-wire visualization (Koca et al., 2018; Genç et al., 2016b; Kirk and Yarusevych, 2017), hot-wire and surface hot-film anemometers (Gomes et al., 2015; Genç et al., 2019; Bhattacharya and Gregory, 2015a, 2015b), temperature-sensitive paint, infrared thermography and liquid crystal (Yorita et al., 2012; Crawford et al., 2013; Fujisawa et al., 2009). Except for these techniques, laser-doppler anemometry (LDA) and PIV experiments were conducted to investigate transition and boundary layer instability phenomena within LSB over the flat plate by Lang et al. (2004).

In what follows, researchers performed flow control studies in order to mitigate the negative effects of LSB. In this respect, flow control methods were classified into two branches: (*i*) active control (Joshi and Bhattacharya, 2019) and (*ii*) passive control (Genç et al., 2020a) techniques. In these days, passive control techniques have been chosen more than active ones since they did not consume external energy. Some of those controllers could be categorized as follows: utilizing the dimple (Roy et al., 2022a), implementing of roughness material (Genç et al., 2019) and vortex generators (VGs) (Li et al., 2019), considering the bio-inspired tubercles (Roy et al., 2022b) and grooves (Seo and Hong, 2016), using the slits (Karasu, 2020), utilizing local flexible membrane (Koca et al., 2022b) investigating the flexible airfoils (Tamai et al., 2008; Gordnier and Attar, 2014; Lian and Shyy, 2007) and so on.

Notwithstanding all studies conducted by the researchers so far, the overall low Reynolds number flow phenomena are still not completely understood because of their unsteady behavior. Hence, numerical and experimental investigations must be performed for a better understanding of the transition inception and the progress of LSB by capturing the instantaneous and time-dependent variations. The lower surface of a Clark-Y airfoil is parallel to its chord line, which allows it to have more

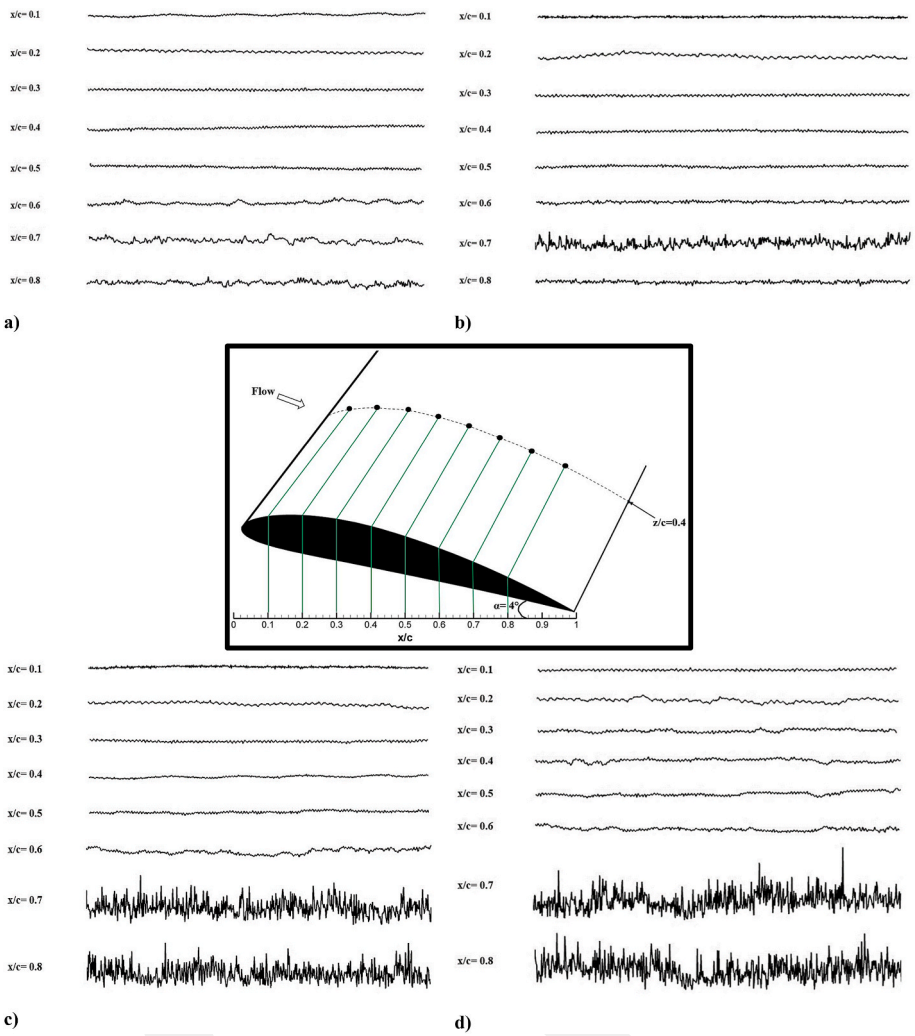

Fig. 5. Time histories of the voltage signals acquired by hot-film sensor on the uncontrolled Clark-Y airfoil, α = 4°, a) Re = 3.5 × 10^4, b) Re = 7 × 10^4, c) Re = 1.05 × 10^5, d) Re = 1.4 × 10^5.

selectable at low speeds. Due to being the pressure (lower) surface parallel to the chord line, it was focused on the low Re number flow and LSB, and its control over the suction (upper) surface of the airfoil. Concerning the novelty of the study, segmented flexible airfoils were investigated numerically (Hefeng et al., 2015). However, there was not any detailed experimental investigation in the literature. It would be the first time in the literature that transition onset, intermittency distribution, as well as LSB formation over the uncontrolled Clark-Y airfoil (without flexible material), were carried out in detail and the control of undesired flow phenomena formed on Clark-Y airfoil was then investigated using the local flexible material (latex rubber sheet) over the suction surface as the controlled case. The determination of flexible membrane location was already investigated in our previous study (Koca et al., 2022a). The most suitable position was determined between x/c = 0.2 and x/c = 0.4.

2. Experimental equipment and data analysis methods

In order to investigate flow phenomena such as boundary layer separation, transition to turbulence, and formation of LSB over Clark-Y airfoil operating at a low Reynolds number regime, the materials, and experimental methods were fulfilled as follows:

2.1. Wind tunnel

All tests were implemented in the suction type and low-speed wind tunnel of the Wind Engineering and Aerodynamic Research Group Laboratory (WEAR) at Erciyes University. This wind tunnel has a ~2.5 m long-closed test section, which is a square with a dimension of 0.5 m × 0.5 m, surrounding it in conjunction with the transparent plexiglass layer to visualize flow phenomena. The free stream velocity in the tunnel can be varied from 3 m/s (TI = 0.91%) to 40 m/s (TI = 0.35%). Each test was characterized by its chord-based Reynolds number, identified as follows:

$$Re = \frac{\rho U_\infty c}{\mu} \tag{1}$$

where μ was the dynamic viscosity and c was the chord length of selected airfoil. U_∞ was the flow velocity in the test facility which was set by adjusting the pressure in the wind tunnel and was then utilized to calculate the velocity by performing the principle of Bernoulli. More technical information with regard to wind tunnel can be seen in Table 1.

2.2. The selected airfoils as specimen

Clark-Y airfoils generally are utilized in steady flow at the regime of low Reynolds number (Marchman, 1984; Raush et al., 2016). Additionally, its lower surface is parallel to its chord line. This allows it to

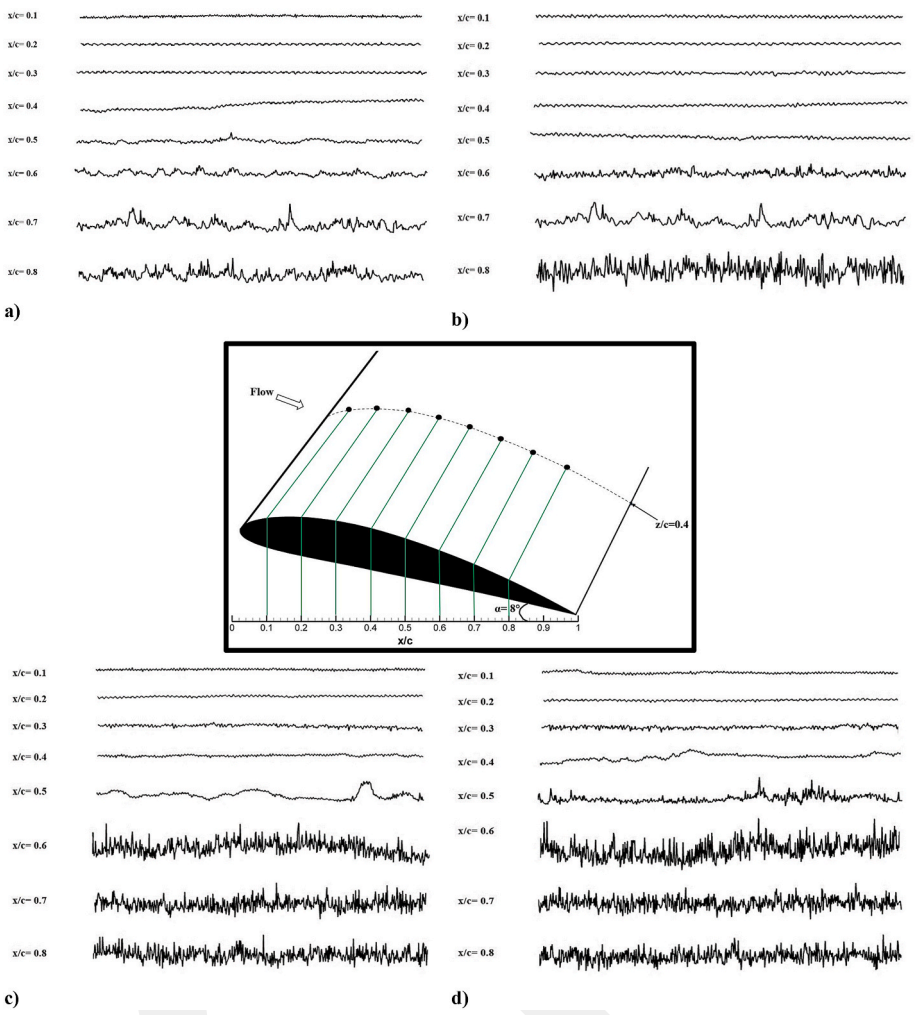

Fig. 6. Time histories of the voltage signals acquired by hot-film sensor on the uncontrolled Clark-Y airfoil, α = 8°, a) Re = 3.5 × 10^4, b) Re = 7 × 10^4, c) Re = 1.05 × 10^5, d) Re = 1.4 × 10^5.

have more stability at low speeds (Houghton and Carpenter, 2003). Being the pressure (lower) surface parallel to the chord line allowed us to focus only on the low Re number flow and LSB, and its control over the suction (upper) surface of the airfoil, therefore, the Clark-Y airfoil was selected as a test specimen. The tests were performed on surfaces of Clark-Y airfoil with 0.2 m chord length and 0.3 m span length. In Fig. 2, the selected airfoil was fabricated by utilizing a 3D printer after the design processes. During manufacturing of the airfoils, the material occupancy rate was selected and employed as ~18% to not have heavier, tough, and bulky airfoils. The fabricated models were firstly rubbed with sandpaper to prevent the roughness effects and dust because of small production residues over the surfaces and their surfaces were then painted with a rapid-drying acrylic spray to obtain a very polished surface. Regarding the technical description of the membrane material, it was a latex rubber sheet, with a thickness of 0.2 mm, Young's modulus (E) of 2.2 MPa, and density of 1 g/cm^3. The latex rubber is an excellent general-purpose material that is suitable for use in a wide range of applications. The high strength and elongation properties of the latex make it particularly popular for use in lining complex shapes as well as textile industries. Finally, both pressure and suction surfaces were covered with membrane material to acquire a homogenous flow structure formed on the airfoil. The latex rubber sheet was glued to the frame of the cavity on the suction surface, as well as all the edges.

2.3. Measurements of aerodynamic force coefficients

As shown in our previous study (Genç et al., 2018, 2020b), the tests for conditions having various flow velocity were conducted using an aerodynamic force measurement system. In order to be able to detect aerodynamic forces, two load cells were utilized (Genç et al., 2018). The calibration was conducted by loading the cell with known weights and was repeated before experiments to ensure consistency. The uncertainty values in the lift and drag force coefficients were 5% and 5.2% at Re = 1 × 10^5, respectively (Genç et al., 2012). Regarding the data recording, they were taken at a sample rate of 1000 Hz for 10 s for whole cases. In what follows, measured forces of F_L and F_D were transformed to the lift (C_L) and drag (C_D) coefficients with equations, respectively:

$$C_L = \frac{2F_L}{\rho U_\infty^2 S} \tag{2}$$

$$C_D = \frac{2F_D}{\rho U_\infty^2 S} \tag{3}$$

where ρ was the air density, S was an area of airfoil suction surface.

2.4. Hot-film (glue-on type) sensors

Another method in terms of detection of transition onset and progress of LSB was an experiment with surface hot-film anemometry.

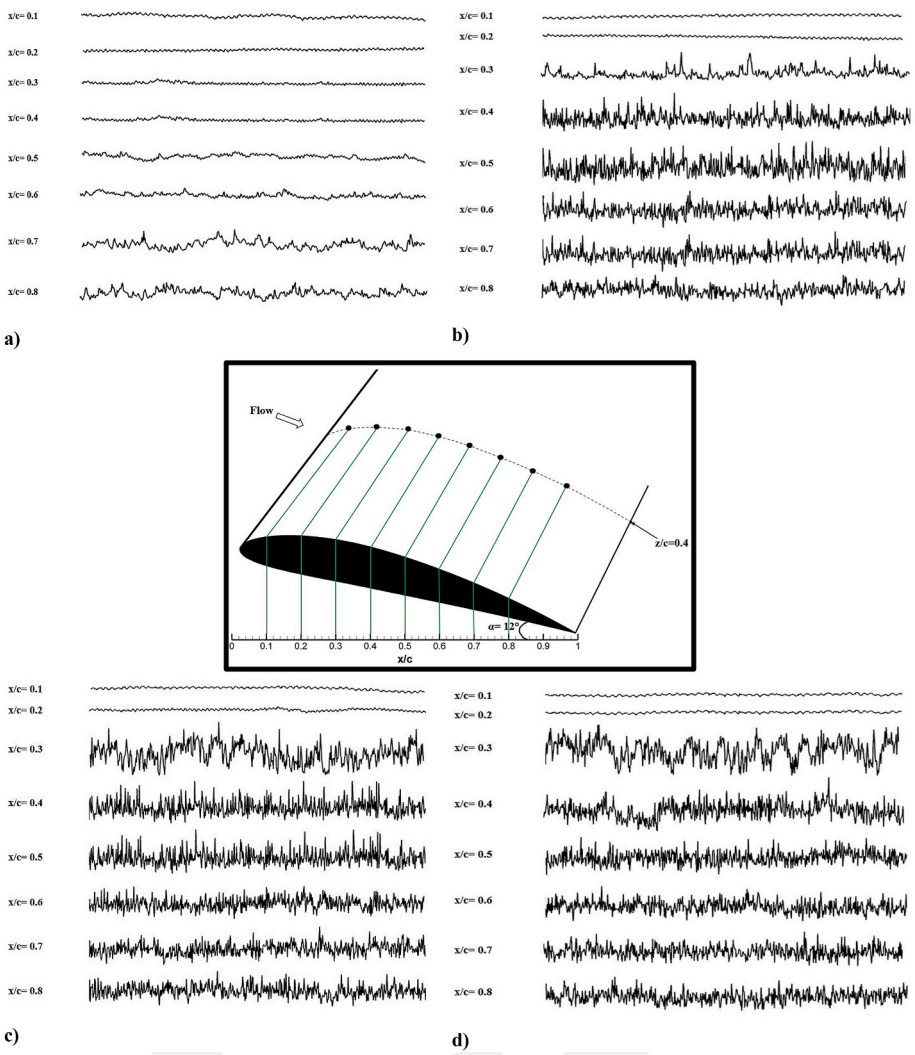

Fig. 7. Time histories of the voltage signals acquired by hot-film sensor on the uncontrolled Clark-Y airfoil, $\alpha = 12^{\circ}$, a) $Re = 3.5 \times 10^4$, b) $Re = 7 \times 10^4$, c) $Re = 1.05 \times 10^5$, d) $Re = 1.4 \times 10^5$.

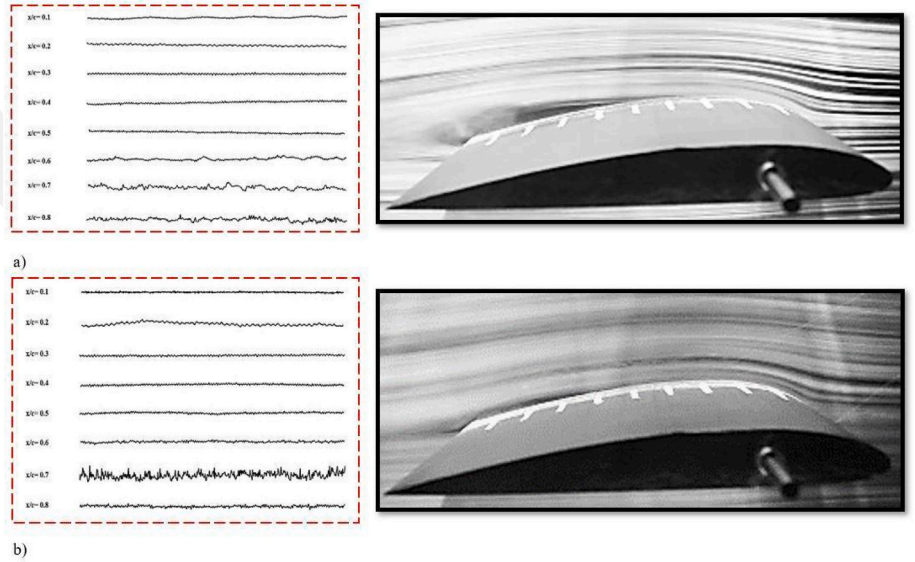

Fig. 8. Comparison of voltage signals with visualization results, $\alpha = 4^{\circ}$, a) time history of voltage signals with instantaneous smoke-wire experiment image at $Re = 3.5 \times 10^4$, b) time history of voltage signals with instantaneous smoke-wire experiment image at $Re = 7 \times 10^4$.

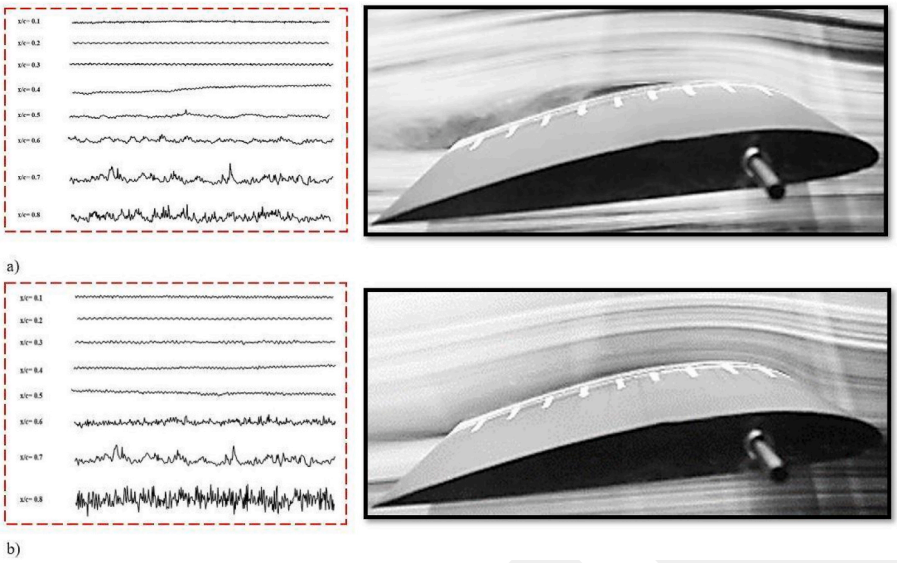

Fig. 9. Comparison of voltage signals with visualization results, α = 8°, a) time history of voltage signals with instantaneous smoke-wire experiment image at Re = 3.5 × 10^4, b) time history of voltage signals with instantaneous smoke-wire experiment image at Re = 7 × 10^4.

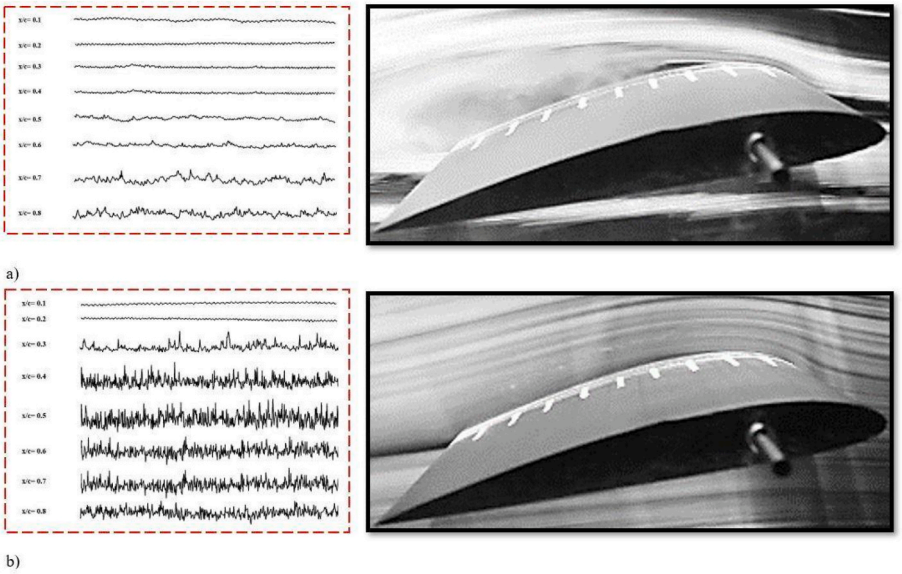

Fig. 10. Comparison of voltage signals with visualization results, α = 12°, a) time history of voltage signals with instantaneous smoke-wire experiment image at Re = 3.5 × 10^4, b) time history of voltage signals with instantaneous smoke-wire experiment image at Re = 7 × 10^4.

Separation and reattachment locations, transition, and turbulence spots could be discovered thanks to this technique in detail. On the other hand, undesired criteria such as sample material caused the calibration of hot-film gauges to be too sophisticated, resulting in this method was rarely performed. In spite of un-calibrated data, semi-measurable information with regard to boundary layer condition were conducted in this study. As technically explained in Fig. 3, a glue-on type (55R47) hot-film gauge was used on the suction surfaces of selected airfoils. The size of the gauge was 8 mm × 1.6 mm and the size of its sensor was 0.1 mm × 0.9 mm. To overlay the gauges on the suction surface, super glue was utilized. The measurement was performed from x/c = 0.1 to x/c = 0.8 with the intervals of 0.1c. A multichannel constant temperature anemometer (CTA) was employed to record data during the test. Furthermore, ~30000 data were sampled for 10 s.

2.5. *Visualizations of flow phenomena with smoke-wire method*

Regarding the visualization of flow phenomena on suction surfaces, the smoke-wire technique was performed with various flow states. As denoted in Fig. 4, the instrumentations and materials of the method were ~0.3 mm thin wire, oil, a heater in order to burn oil droplets, three illustrators, and a camera to capture the smoke sheets. From the past experiences of the authors, there were two reasons in terms of choosing ~0.3 mm thin wire, (*i*) the most suitable smoke sheets formed along the chord-wise and (*ii*) the oil dispersed very well. Copper wire was vertically positioned in front of the airfoil. The distance between the wire and the airfoil was ~1.5c. That distance caused the smoke sheets to be uniform and stringy. Forming the oil droplet along the wire was manually performed by dribbling. The heater was conducted at a level of 3 mA to burn oil on the wire. Then, sheets coming from burned wire were visualized by using halogens. For better-quality images,

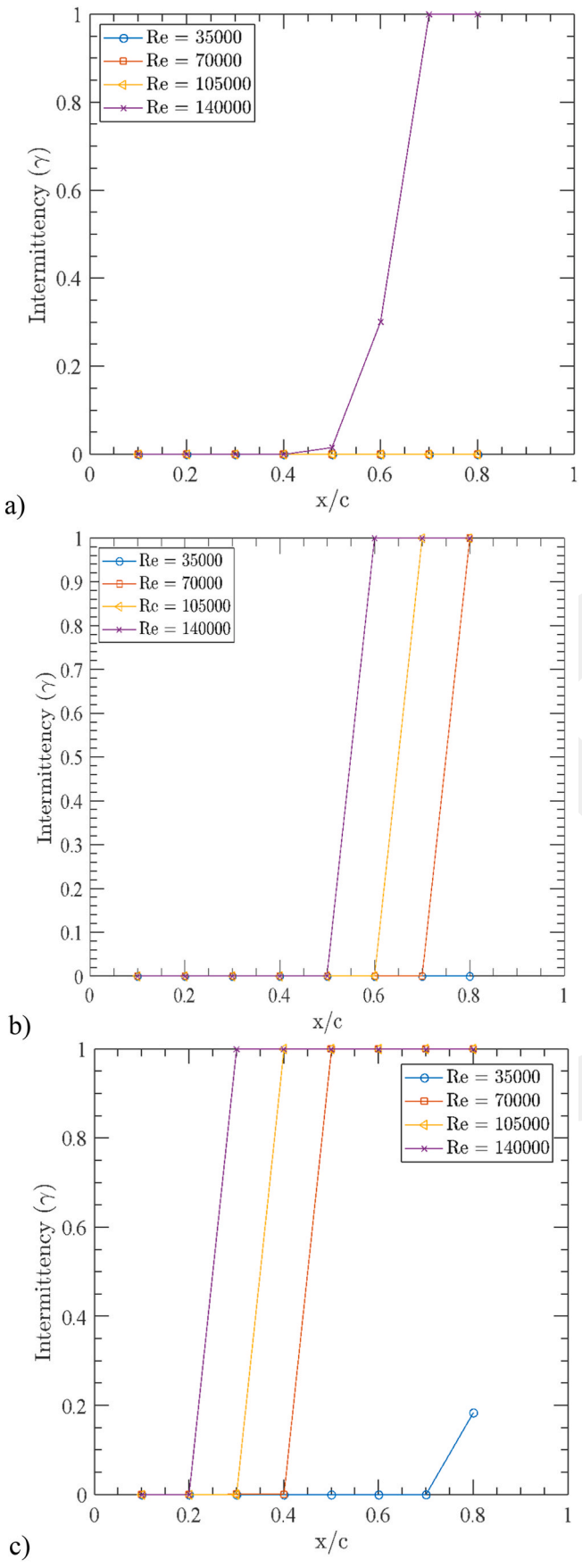

Fig. 11. The intermittency graphs, a) $\alpha = 4^{\circ}$, b) $\alpha = 8^{\circ}$, c) $\alpha = 12^{\circ}$.

measurements were repeated two times. To capture the videos of smoke sheets, a camera was positioned near the test chamber. After the test, every obtained video was divided into 1000 frames to capture smoke sheets by post-processing the experiment. The best quality frames were then selected from these 1000 frames. Regarding the technical specification of Nikon camera, the sensor and display resolutions were 24 MP CMOS and 1.04 M-dot vary-angle which ensured to capture of more high-definition smoke sheets.

3. Results and discussion

3.1. Analysis of voltage signals from individual hot-film sensors

Figs. 5–7 illustrated the voltage signals measured by hot-film sensors for $\alpha = 4^{\circ}$, $\alpha = 8^{\circ}$ and $\alpha = 12^{\circ}$, respectively. Although these data only represented the un-calibrated voltage signals acquired by the hot-film sensors, they nicely demonstrated the salient LSB flow phenomena and transition onset over the suction surface of uncontrolled Clark-Y airfoil. At $\alpha = 4^{\circ}$, the amplitude of fluctuations from $x/c = 0.1$ to $x/c = 0.4$ was low at Reynolds number of 3.5×10^4 and 7×10^4, indicating presence of laminar flow. That results agreed with the results measured by microphone (zçakmak et al., 2019), piezoelectric (Stuber et al., 2021) and hot-film signals (Gardner and Richter, 2015). Additionally, it was clearly observed that the amplitude of fluctuations from $x/c = 0.6$ to $x/c = 0.8$ increased. This implied that the formation of LSB and transition occurred in this region. In Fig. 5 (b), it was observed that the fluctuation at $x/c = 0.7$ was higher than that of $x/c = 0.8$. The reason behind that the flow in the boundary layer was too unsteady in that point. Increasing Reynolds number to 1.05×10^5 and 1.4×10^5 caused the amplitude of fluctuations to change. In particular, the flow was comparatively stable until $x/c = 0.6$, while its amplitude of fluctuation increased with the sharp peaks at $x/c = 0.7$ and $x/c = 0.8$. At $\alpha = 8^{\circ}$ and $Re = 3.5 \times 10^4$, the amount of fluctuation was comparatively low from $x/c = 0.1$ to $x/c = 0.4$, indicating that the flow was at laminar regime. Until $x/c = 0.6$, a spiky signal was not observed at $Re = 7 \times 10^4$. Then, the amplitude of fluctuations gradually increased downstream of $x/c = 0.6$. At $Re = 1.05 \times 10^5$ and $Re = 1.4 \times 10^5$, the amplitude of fluctuations was higher than those occurring at lower Reynolds numbers. These high amplitude fluctuations confirmed the behavior of the turbulent boundary layer, complying with the findings by Ducoin et al. (2012). Furthermore, the highest amplitude fluctuations were observed as the angle of attack was raised to $\alpha = 12^{\circ}$. Most probably, LSB-induced vortex shedding caused the highest amplitude fluctuations to occur at a higher angle of attack as confirmed in the studies (Ducoin et al., 2016; Ducoin and Astolfi, 2019).

3.2. Intermittency analysis of voltage signals

In wall-bounded shear flows, intermittent flow behavior was observed, which was central to the process of transition from laminar to turbulent flow. Detailed information with regards to transition onset, formation of the LSB, and fully turbulent regime may be understood thanks to intermittency values. Intermittency dispersion in the transitional boundary layer can be identified as the fraction of time the flow remains turbulent in the flow field, and its value varies between $\gamma = 0$ and $\gamma = 1$. There are several methods available in the literature to determine the intermittency distribution, and it is briefly reviewed in Veerasamy and Atkin (2020) and Veerasamy et al. (2021). Further, a common procedure has been adopted for all the methods, consisting of three sequential steps: (*i*) Detector function - detects intermittent turbulent spots by sensitizing the signal; (*ii*) Criterion function - smooths the sensitized signal particularly to avoid laminar spikes; (*iii*) Indicator function - by choosing an appropriate threshold value, laminar and turbulent regimes in the transitional flow are indicated with values of $\gamma = 0$ and $\gamma = 1$. Finally, by averaging the indicator function over a given period of time intermittency will be obtained. Among these three steps, a technique to determine a threshold value determines the quality of the

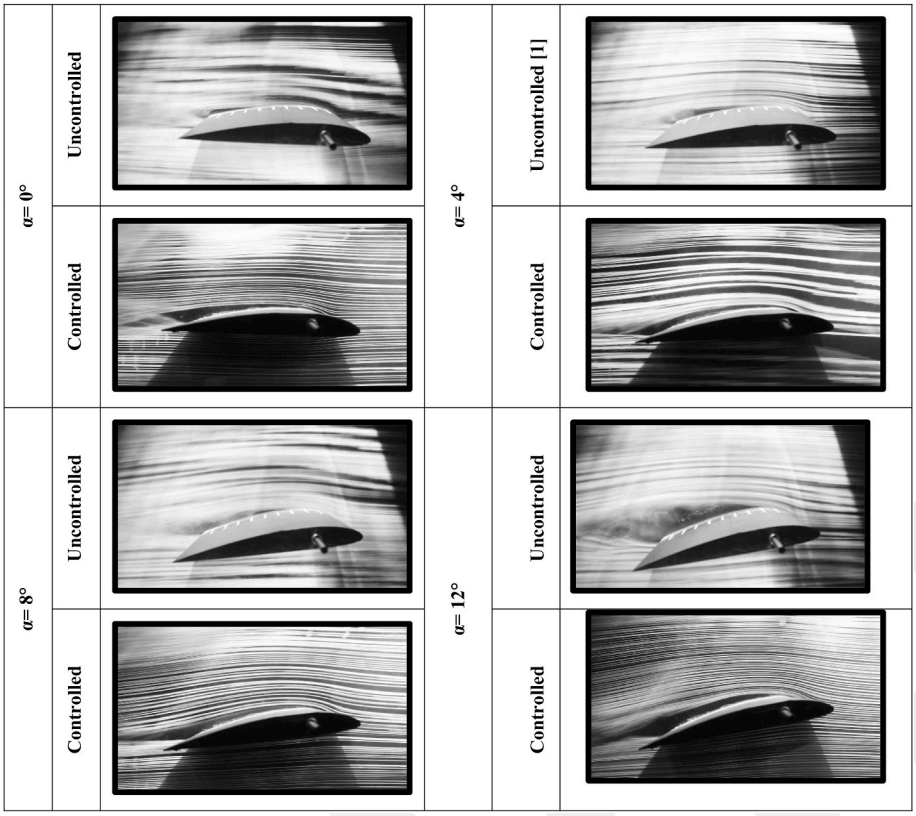

Fig. 12. Comparative instantaneous smoke-wire visualization images of both the uncontrolled and the controlled Clark-Y airfoils, Re = 3.5×10^4.

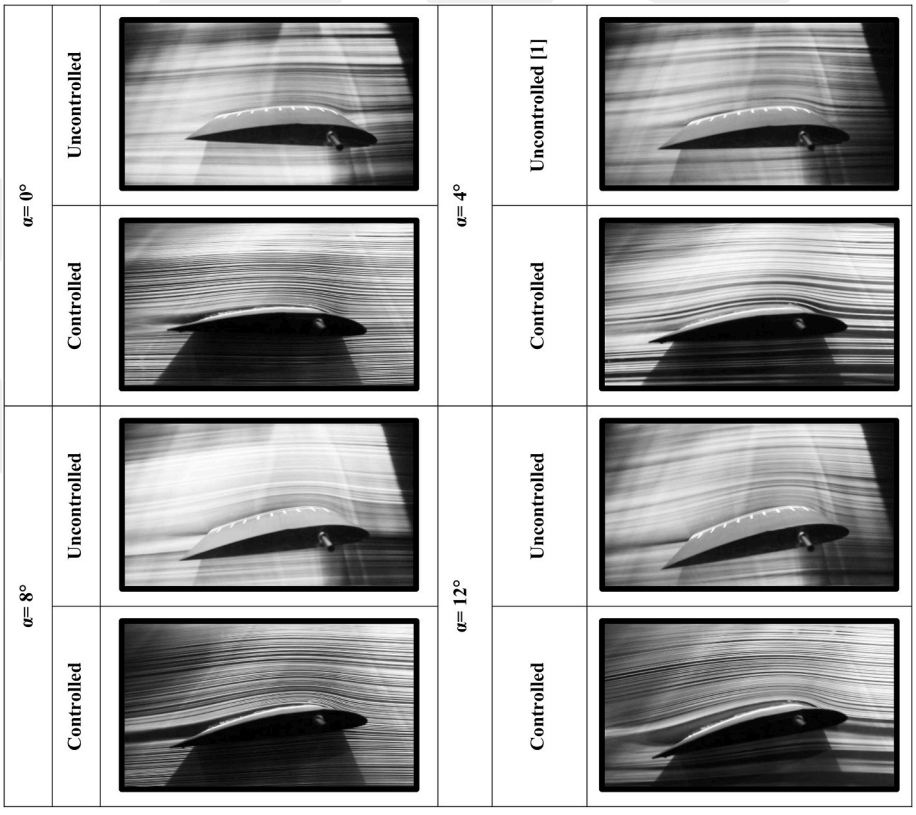

Fig. 13. Comparative instantaneous smoke-wire visualization images of both the uncontrolled and the controlled Clark-Y airfoils, Re = 7×10^4.

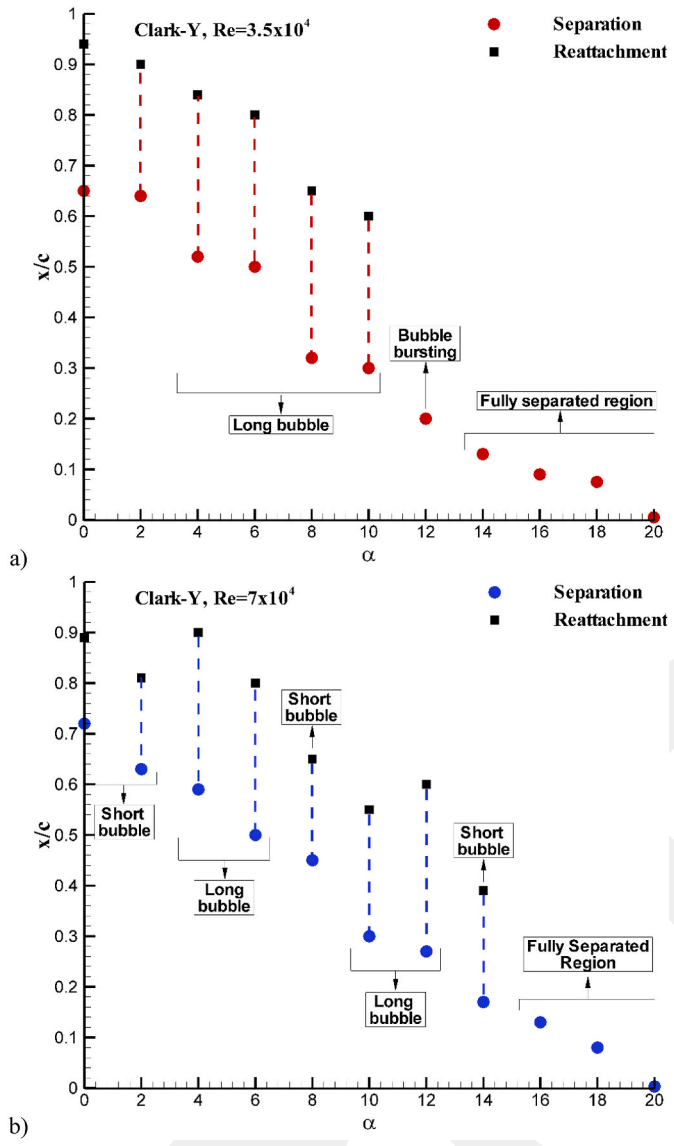

Fig. 14. Location and length of LSB over surface of the uncontrolled Clark-Y airfoil, a) Re = 3.5 × 10^4, b) Re = 7 × 10^4.

intermittency distribution. In this paper, a dual-slope technique proposed by Kuan and Wang (1990) is used for determining the threshold value. In this technique, a probability distribution function (pdf) of the sensitized signal will be plotted against the values of the detector function, and the plot where the two different slopes intersect is considered a threshold value. Based on that, intermittency distribution arrived.

In this respect, firstly, the voltage signals were compared with the visualization results to better understand Figs. 8–10. Then, the intermittency values calculated by voltage signals were illustrated in Fig. 11. Intermittency was plotted as a function of all operating points chordwise. As seen in the graphs, the values for γ = 0 and γ = 1 were blanked. Interestingly, at α = 4°, transition to turbulence was completed inside the investigated region only for the highest Reynolds number (Re = 1.4 × 10^5). Except for intermittency belonging to Re = 1.4 × 10^5, they were all low, indicating that the transition to turbulence was not completed inside the investigated region (the flow on the airfoil). As shown in the images of the smoke-wire visualization, the formation of LSB occurred close to the trailing edge of the airfoil. This may imply two results: (*i*) either transition to turbulence occurred downstream of x/c = 0.8 where could not be measured because of the obstacle of utilizing the hot-film sensor, (*ii*) or transition to turbulence existed in the wake region as seen in examples of the cylinder (Ong and Wallace, 1996) and sphere (Wu and Faeth, 1993). As mentioned in the study with regards to reverse flow inside LSB (Embacher and Fasel, 2014; Rodríguez et al., 2013), it was clearly observed that hot-film signals were absolutely unstable at x/c = 0.5, indicating that the boundary layer was disturbed because of the presence of reverse flow inside LSB.

3.3. Comparison of smoke-wire visualization results

The comparative results of visualization belonging to both uncontrolled and controlled Clark-Y airfoil were presented for Re = 3.5 × 10^4 and Re = 7 × 10^4 in Figs. 12 and 13, respectively. As seen in Fig. 12, it was clearly pointed out that the formation of LSB appeared on the trailing edge of the airfoil at α = 0°. It was observed that a bubble formed at the trailing edge at low angles of attack, and the bubble approached the leading edge with increasing the angle of attack. Due to the nature of the low Reynolds number flow, the separation bubble was especially long bubble formation at Re = 3.5 × 10^4. After α = 4°, this long bubble increased its effectiveness with the increase of the angle of attack. As expected, LSB moved toward the leading edge as the angle of attack was increased at 4° intervals. Moreover, it was clearly seen that the bubble burst nearly the leading edge when the angle of attack was α = 12°, resulting in presence of leading-edge flow separation. In Fig. 13,

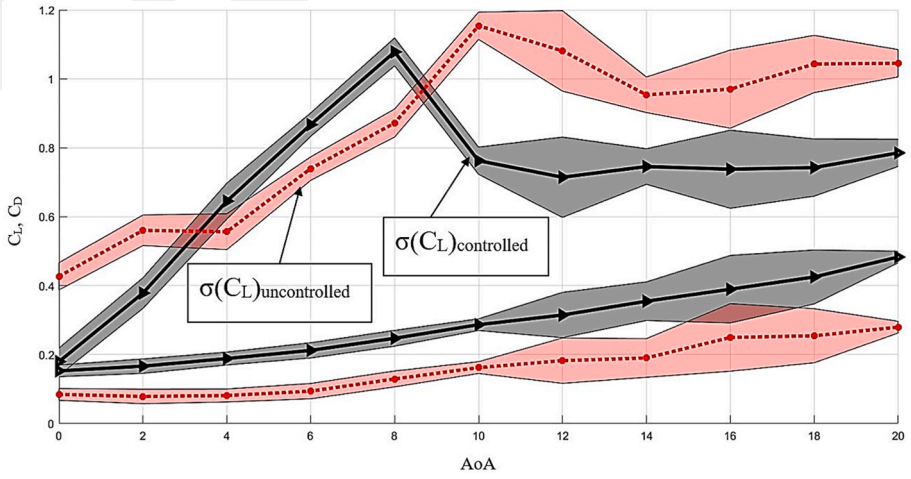

Fig. 15. Fluctuation density results in aerodynamic force coefficients of uncontrolled and controlled Clark-Y airfoils, gray straight line: controlled case, red dotted line: uncontrolled case, Re = 3.5 × 10^4. (For interpretation of the references to colour in this figure legend, the reader is referred to the Web version of this article.)

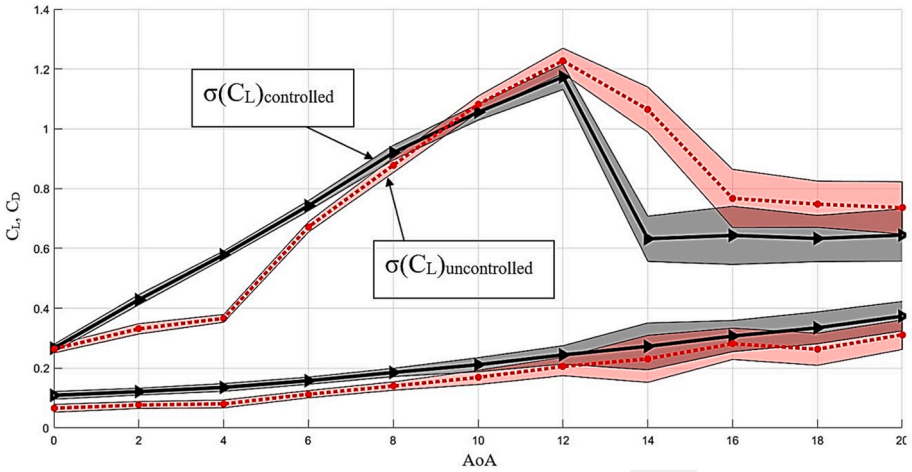

Fig. 16. Fluctuation density results in aerodynamic force coefficients of uncontrolled and controlled Clark-Y airfoils, gray straight line: controlled case, red dotted line: uncontrolled case, Re $= 7 \times 10^{4.}$ (For interpretation of the references to colour in this figure legend, the reader is referred to the Web version of this article.)

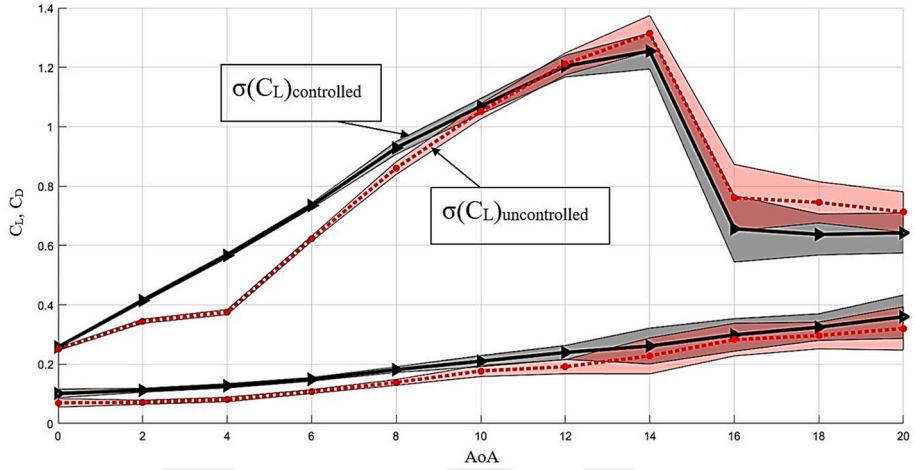

Fig. 17. Fluctuation density results in aerodynamic force coefficients of uncontrolled and controlled Clark-Y airfoils, gray straight line: controlled case, red dotted line: uncontrolled case, Re $= 1.05 \times 10^{5.}$ (For interpretation of the references to colour in this figure legend, the reader is referred to the Web version of this article.)

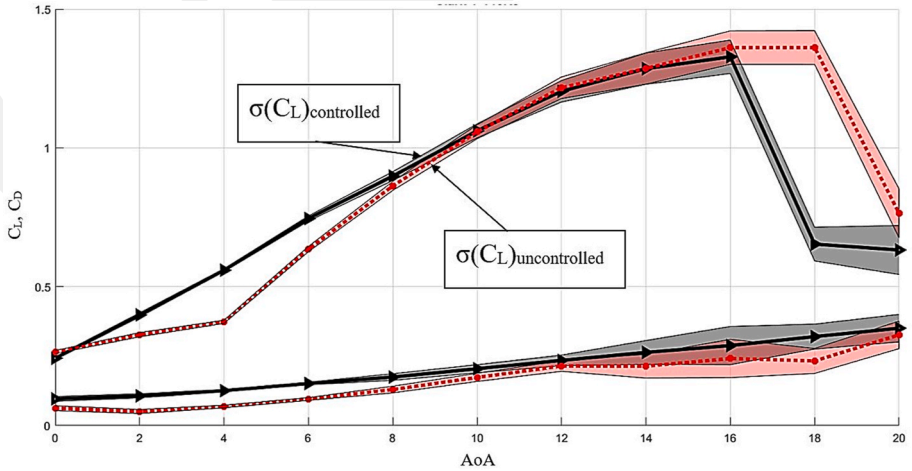

Fig. 18. Fluctuation density results in aerodynamic force coefficients of uncontrolled and controlled Clark-Y airfoils, gray straight line: controlled case, red dotted line: uncontrolled case, Re $= 1.4 \times 10^{5.}$ (For interpretation of the references to colour in this figure legend, the reader is referred to the Web version of this article.)

dominant inertial forces with increasing Reynolds number caused viscous forces to decrease, resulting in a shrinking of the size of LSB. For all cases where LFM was employed on the Clark-Y airfoil, it was obviously illustrated that either the size of LSB was decreased or it was completely suppressed. Additionally, the width of the wake region of the controlled airfoil was narrower than the uncontrolled airfoil. This also clearly implied that LSB-induced eddies and their effects decreased, resulting in the formation more stable flow region in the wake.

Fig. 14 revealed the location and length of LSB over the surface of the uncontrolled Clark-Y airfoil at $Re = 3.5 \times 10^4$ and $Re = 7 \times 10^4$, while Figs. 15–18 demonstrated the aerodynamic force coefficient results for both cases at various Reynolds number. In Fig. 14, changes in the separation and reattachment points formed on the uncontrolled Clark-Y airfoil at low Reynolds number flows according to the results of smoke tests were observed. In these changes, it was observed that a bubble formed at the trailing edge at low angles of attack, and this bubble approached the leading edge with increasing the angle of attack. Due to the nature of the low Reynolds number flow, the separation bubble was especially long bubble formation at $Re = 3.5 \times 10^4$. After $\alpha = 4^\circ$, this long bubble increased its effectiveness with the increase of the angle of attack, and the increase in this effectiveness was manifested by the loss of linearity (straightness of the curve) of the curve in the strength curve in Fig. 15. In addition, as seen from the lines showing the fluctuations of the force results in Fig. 15, fluctuations increased especially due to the presence of the bubble. With the formation of unsteady flow states with the long bubble, fluctuations were clearly observed in the force graphs. These fluctuations caused unsteady forces to occur on the airfoil, and this could also affect the fatigue life of the wing as there were repetitive forces. After $\alpha = 10^\circ$, as illustrated in the smoke-wire graph $\alpha = 12^\circ$ and in Fig. 11, the long bubble burst and the flow would not reattach. Since bubble bursting was a time-dependent flow condition, it caused a peak in force fluctuations in the force graphs. In this study, the main goal was to employ the LFM in order to control the nonlinear behavior and unsteady flow conditions formed by the separation bubble. Similarly, in Fig. 14(b), the situation of the flow on the airfoil with changing of the angle of attack $Re = 7 \times 10^4$ was observed. It was clearly pointed out the LSB was relatively smaller and shorter since Reynolds number and inertia forces increased. With the stability brought by the inertia force, it was seen in Figs. 16–18 that the stall in an uncontrolled case was in the form of a mild stall. In addition, due to the long bubble at $Re = 7 \times 10^4$, $Re = 1.05 \times 10^5$, and $Re = 1.4 \times 10^5$, the aerodynamic performance of the airfoil decreased and the straightness of the lift curve deteriorated at $2^\circ \leq \alpha \leq 8^\circ$. In these graphs, it was revealed that the flow was more stable than $Re = 3.5 \times 10^4$ and the force fluctuations decreased as a result of this stability.

Regarding the averaged force results, the red dotted line indicated the results of the uncontrolled case, while the results of the controlled case were presented as the gray straight line. In addition, the shaded areas which were symbolized as 'σ' pointed out the aerodynamic force fluctuations with time. It was seen that employing LFM over suction surface ensured remarkable effect at pre-stall conditions due to the control of the LSB in terms of enhancing aerodynamic performance for all Reynolds number. That is, it could be said that the positive effects could be revealed especially at $2^\circ \leq \alpha \leq 8^\circ$. From the whole figures, it was obviously seen that there was the skewness on the lift curves of the uncontrolled airfoils. As illustrated from the results of instantaneous smoke-wire visualization, the LSB-induced vibration most probably caused the skewness on the lift curves to form in the uncontrolled case. However, the unsteady flow structures inside of LSB clearly suppressed when LFM was utilized over suction surface, resulting in obtaining a more stable lift curve at the aforementioned angles of attack ranges.

4. Conclusion

Taking LFM as the research object on Clark-Y airfoil was the first and pioneering research in the literature which dealt with the passive control techniques. In this study, the objective is to determine flow phenomena in detail and to investigate the effects of LFM mounted on leading-edge over the suction surface of Clark-Y airfoil. In this respect, first of all, the flow phenomena, which affected the wind/hydro turbine blades aerodynamically, were experimentally examined on the Clark-Y airfoil in detail. In what follows, the LFM was employed between $x/c = 0.2$ and $x/c = 0.4$ of the suction surfaces in order to observe how it affected flow pattern and to understand the flow-induced passive oscillation with a flexible membrane. Finally, the results of both uncontrolled and controlled Clark-Y airfoils were compared with each other. Through comparative analysis, the conclusions were drawn as follows:

1) The detailed intermittency analysis from the glue-on probe revealed that the transition to turbulence and LSB formed close to the trailing edge, and those moved towards the leading edge when increasing the angle of attack. In addition, as expectedly, the size of LSB diminished with the increment of inertial forces when Reynolds number increased simultaneously.
2) The results of both aerodynamic force measurement and 2-D smoke-wire flow visualization belonging to the uncontrolled Clark-Y airfoil revealed the progress of LSB at moderate angles of attack and leading-edge flow separation at higher angles of attack negatively affected airfoil stability by ensuring extra fluctuation at both lift and drag curves.
3) It was clearly observed that the aerodynamic performance enhanced at moderate angles of attack when employing the LFM over the suction surface. Additionally, at the pre- and the post-stall regions, the fluctuations at lift curves especially at higher Reynolds numbers were enormously mitigated.

All showed that a more stable airfoil aerodynamic performance which produced less vibration, and less noise could be obtained by means of flow-induced passive oscillation with LFM at the local surface of the airfoil, hereby the turbine blade stability could be increased.

CRediT authorship contribution statement

Kemal Koca: Methodology, Investigation, Data curation, Formal analysis, Validation, Writing – original draft. **Mustafa Serdar Genç:** Project administration, Conceptualization, Methodology, Investigation, Supervision, Writing – review & editing. **Dhamotharan Veerasamy:** Formal analysis. **Mustafa Özden:** Investigation, Data curation.

Declaration of competing interest

The authors declare that they have no known competing financial interests or personal relationships that could have appeared to influence the work reported in this paper.

Data availability

No data was used for the research described in the article.

Acknowledgement

The authors thank the Scientific Research Projects Unit of Erciyes University under the contract numbers: FDK-2019-8726 for funding, and also thank the Scientific and Technological Research Council of Turkey (TÜBİTAK) for the Doctoral Scholarship for Priority Areas 2211/C for the author Kemal KOCA.

Nomenclature

Abbreviation

LSB	Laminar separation bubble
LFM	Local flexible membrane

VGs	Vortex generators
APG	Adverse pressure gradient
2-D	Two dimensional
CTA	Constant temperature anemometer
AoA	Angle of attack
PIV	Particle image velocimetry
LDA	Laser doppler anemometry
RANS	Reynolds Averaged Naiver Stokes
LES	Large Eddy Simulation
DNS	Direct Numerical Simulation
SST	Shear Stress Transport
T-S	Tollmien-Schlichting

Subscripts

L	Lift
D	Drag
max	Maximum
∞	Infinity

Symbols

Re	Reynolds number
c	Chord length (mm)
μ	Dynamic viscosity (kg/m.s)
S	Area of airfoil surface (mm^2)
γ	Intermittency value
F_L	Lift force (N)
F_D	Drag force (N)
C_L	Lift coefficient
C_D	Drag coefficient
U_∞	Free stream velocity (m/s)
α	Angle of attack (deg.)
E	Young's modulus (E)
Tu	Turbulence level
σ	Standard deviation
ρ	Air density (kg/m^3)
ρ_m	Flexible membrane density (g/cm^3)

References

Açıkel, H.H., Genç, M.S., 2016. Flow control with perpendicular acoustic forcing on NACA 2415 aerofoil at low Reynolds numbers. Proc IMechE, Part G- Journal of Aerospace Engineering 230, 2447–2462.

Bhattacharya, S., Ahmed, A., 2020. Effect of aspect ratio on the flow over a wall-mounted hemispherical turret. Int. J. Heat Fluid Flow 84, 108600.

Bhattacharya, S., Gregory, J.W., 2015a. Effect of three-dimensional plasma actuation on the wake of a circular cylinder. AIAA J. 53 (4), 958–967.

Bhattacharya, S., Gregory, J.W., 2015b. Investigation of the cylinder wake under spanwise periodic forcing with a segmented plasma actuator. Phys. Fluids 27 (1), 014102.

Bhattacharya, S., Gregory, J.W., 2018. Optimum-wavelength forcing of a bluff body wake. Phys. Fluids 30 (1), 015101.

Bhattacharya, S., Gregory, J.W., 2020. The effect of spatially and temporally modulated plasma actuation on cylinder wake. AIAA J. 58 (9), 3808–3818.

Crawford, B.K., Duncan Jr., G.T., West, D.E., Saric, W.S., 2013. Laminar-turbulent boundary layer transition imaging using ir thermography. Opt Photon. J. 3 (3), 233.

Ducoin, A., Astolfi, J.A., 2019. Wall-pressure fluctuations of laminar separation bubble based on direct numerical simulation and experiments over a hydrofoil at Re= 450,000. Eur. J. Mech. B Fluid 76, 132–144.

Ducoin, A., Astolfi, J.A., Gobert, M.L., 2012. An experimental study of boundary-layer transition induced vibrations on a hydrofoil. J. Fluid Struct. 32, 37–51.

Ducoin, A., Loiseau, J.C., Robinet, J.C., 2016. Numerical investigation of the interaction between laminar to turbulent transition and the wake of an airfoil. Eur. J. Mech. B Fluid 57, 231–248.

Durbin, P.A., 2002. DNS of Bypass Transition. Closure Strategies for Turbulent and Transitional Flows.

Embacher, M., Fasel, H.F., 2014. Direct numerical simulations of laminar separation bubbles: investigation of absolute instability and active flow control of transition to turbulence. J. Fluid Mech. 747, 141–185.

Fujisawa, N., Oguma, Y., Nakano, T., 2009. Measurements of wall-shear-stress distribution on an NACA0018 airfoil by liquid-crystal coating and near-wall particle image velocimetry (PIV). Meas. Sci. Technol. 20 (6), 065403.

Galbraith, M., Visbal, M., 2008. Implicit large eddy simulation of low Reynolds number flow past the SD7003 airfoil. In: 46th AIAA Aerospace Sciences Meeting and Exhibit, p. 225.

Gardner, A.D., Richter, K., 2015. Boundary layer transition determination for periodic and static flows using phase-averaged pressure data. Exp. Fluid 56 (6), 1–13.

Gaster, M., 1966. The structure and behaviour of laminar separation bubbles. AGARD CP 4, 813–854.

Genç, M., Lock, G., Kaynak, Ü., 2008. An Experimental and Computational Study of Low Re Number Transitional Flows over an Aerofoil with Leading Edge Slat. The 26th Congress of ICAS and 8th AIAA ATIO, p. 8877.

Genç, M.S., Kaynak, Ü., Yapici, H., 2011. Performance of transition model for predicting low Re aerofoil flows without/with single and simultaneous blowing and suction. Eur. J. Mech. B Fluid 30.2, 218–235.

Genç, M.S., Karasu, İ., Açıkel, H.H., 2012. An experimental study on aerodynamics of NACA2415 aerofoil at low Re numbers. Exp. Therm. Fluid Sci. 39, 252–264.

Genç, M.S., Açıkel, H.H., Akpolat, M.T., Özkan, G., Karasu, İ., 2016a. Acoustic control of flow over NACA 2415 aerofoil at low Reynolds numbers. Journal of Aerospace Engineering-ASCE 29 (6), 04016045.

Genç, M.S., Koca, K., Açıkel, H.H., Özkan, G., Kiriş, M.S., Yildiz, R., 2016b. Flow characteristics over NACA4412 airfoil at low Reynolds number. In: EPJ Web of Conferences. EDP Sciences, 02029.

Genç, M.S., Özkan, G., Özden, M., Kiriş, M.S., Yildiz, R., 2018. Interaction of tip vortex and laminar separation bubble over wings with different aspect ratios under low Reynolds numbers. Proc. IME C J. Mech. Eng. Sci. 232 (22), 4019–4037.

Genç, M.S., Koca, K., Açıkel, H.H., 2019. Investigation of pre-stall flow control on wind turbine blade airfoil using roughness element. Energy 176, 320–334.

Genç, M.S., Koca, K., Demir, H., Açıkel, H.H., 2020a. Traditional and New Types of Passive Flow Control Techniques to Pave the Way for High Maneuverability and Low Structural Weight for UAVs and MAVs. Autonomous Vehicles, pp. 131–160.

Genç, M.S., Açıkel, H.H., Koca, K., 2020b. Effect of partial flexibility over both upper and lower surfaces to flow over wind turbine airfoil. Energy Convers. Manag. 219, 113042.

Gomes, R.A., Stotz, S., Blaim, F., Niehuis, R., 2015. Hot-film measurements on a low-pressure turbine linear cascade with bypass transition. J. Turbomach. 137, 9.

Gordnier, R.E., Attar, P.J., 2014. Impact of flexibility on the aerodynamics of an aspect ratio two membrane wing. J. Fluid Struct. 45, 138–152.

Hain, R., Kähler, C.J., Radespiel, R., 2009. Dynamics of laminar separation bubbles at low-Reynolds-number aerofoils. J. Fluid Mech. 630, 129.

Hefeng, D., Chenxi, W., Shaobin, L., Zhen, S.X., 2015. Numerical research on segmented flexible airfoils considering fluid-structure interaction. Procedia Eng. 99, 57–66.

Houghton, E.L., Carpenter, P.W., 2003. Aerodynamics for Engineering Students. Elsevier.

Istvan, M.S., Yarusevych, S., 2018. Effects of free-stream turbulence intensity on transition in a laminar separation bubble formed over an airfoil. Exp. Fluid 59 (3), 52.

Jagadeesh, C.S., Balthazar, M., Gross, A., Fasel, H.F., 2013. Experimental investigation of the structure and dynamics of laminar separation bubbles at the onset of bursting. In: 31st AIAA Applied Aerodynamics Conference, p. 3195.

Joshi, K., Bhattacharya, S., 2019. Large-eddy simulation of the effect of distributed plasma forcing on the wake of a circular cylinder. Comput. Fluid 193, 104295.

Karasu, İ., 2020. Flow control over a diamond-shaped cylinder using slits. Exp. Therm. Fluid Sci. 112, 109992.

Karasu, İ., Özden, M., Genç, M.S., 2018. Performance assessment of transition models for three-dimensional flow over NACA4412 wings at low Reynolds numbers. J. Fluid Eng. 140, 12.

Kirk, T.M., Yarusevych, S., 2017. Vortex shedding within laminar separation bubbles forming over an airfoil. Exp. Fluid 58 (5), 43.

Koca, K., Genç, M.S., Açıkel, H.H., Çağdaş, M., Bodur, T.M., 2018. Identification of flow phenomena over NACA 4412 wind turbine airfoil at low Reynolds numbers and role of laminar separation bubble on flow evolution. Energy 144, 750–764.

Koca, K., Genç, M.S., Özkan, R., 2021. Mapping of laminar separation bubble and bubble-induced vibrations over a turbine blade at low Reynolds numbers. Ocean Eng. 239, 109867.

Koca, K., Genç, M.S., Bayır, E., Soğuksu, F.K., 2022a. Experimental study of the wind turbine airfoil with the local flexibility at different locations for more energy output. Energy 239, 121887.

Koca, K., Genç, M.S., Ertürk, S., 2022b. Impact of local flexible membrane on power efficiency stability at wind turbine blade. Renew. Energy 197, 1163–1173.

Kuan, C.L., Wang, T., 1990. Investigation of the intermittent behavior of transitional boundary layer using a conditional averaging technique. Exp. Therm. Fluid Sci. 3 (2), 157–173.

Lang, M., Rist, U., Wagner, S., 2004. Investigations on controlled transition development in a laminar separation bubble by means of LDA and PIV. Exp. Fluid 36 (1), 43–52.

Li, X.K., Liu, W., Zhang, T.J., Wang, P.M., Wang, X.D., 2019. Experimental and numerical analysis of the effect of vortex generator installation angle on flow separation control. Energies 12 (23), 4583.

Lian, Y., Shyy, W., 2007. Laminar-turbulent transition of a low Reynolds number rigid or flexible airfoil. AIAA J. 45 (7), 1501–1513.

Marchman, J., 1984. Clark-Y airfoil performance at low Reynolds numbers. In: 22nd Aerospace Sciences Meeting, p. 52.

Ong, L., Wallace, J., 1996. The velocity field of the turbulent very near wake of a circular cylinder. Exp. Fluid 20 (6), 441–453.

Raush, G., Castilla, R., Gamez-Montero, P.J., Wojciechowski, J., Codina, E., 2016. Flexible rod design for educational wind balance. Exp. Tech. 40 (1), 111–119.

Rodríguez, D., Gennaro, E.M., Juniper, M.P., 2013. The two classes of primary modal instability in laminar separation bubbles. J. Fluid Mech. 734.

Roy, S., Biswas, A., Das, B., Reddy, B.V., 2022a. Flow control of a wind-turbine airfoil with a leading-edge spherical dimple. Int. J. Green Energy 1–19.

Roy, S., Das, B., Biswas, A., 2022b. A comprehensive review of the application of bio-inspired tubercles on the horizontal axis wind turbine blade. Int. J. Environ. Sci. Technol. 1–28.
Schülein, E., 2004. Development and application of the thin oil film technique for skin friction measurements in the short-duration hypersonic wind tunnel. In: New Results in Numerical and Experimental Fluid Mechanics IV. Springer, Berlin, Heidelberg, pp. 407–414.
Seo, S.H., Hong, C.H., 2016. Performance improvement of airfoils for wind blade with the groove. Int. J. Green Energy 13 (1), 34–39.
Stuber, V.L., Kotsonis, M., van der Zwaag, S., 2021. Boundary layer state detection using piezoelectric sensors. Smart Mater. Struct. 31 (1), 015014.
Tamai, M., Murphy, J., Hu, H., 2008. An experimental study of flexible membrane airfoils at low Reynolds numbers. In: 46th AIAA Aerospace Sciences Meeting and Exhibit, p. 580.
Veerasamy, D., Atkin, C., 2020. A rational method for determining intermittency in the transitional boundary layer. Exp. Fluid 61 (1), 1–13.
Veerasamy, D., Atkin, C.J., Ponnusami, S.A., 2021. Aerofoil wake-induced transition characteristics on a flat-plate boundary layer. J. Fluid Mech. 920.
Windte, J., Scholz, U., Radespiel, R., 2006. Validation of the RANS-simulation of laminar separation bubbles on airfoils. Aero. Sci. Technol. 10 (6), 484–494.
Wolf, E., Kähler, C.J., Troolin, D.R., Kykal, C., Lai, W., 2011. Time-resolved volumetric particle tracking velocimetry of large-scale vortex structures from the reattachment region of a laminar separation bubble to the wake. Exp. Fluid 50 (4), 977–988.
Wu, J.S., Faeth, G.M., 1993. Sphere wakes in still surroundings at intermediate Reynolds numbers. AIAA J. 31 (8), 1448–1455.
Yorita, D., Asai, K., Klein, C., Henne, U., Schaber, S., 2012. Transition detection on rotating propeller blades by means of temperature sensitive paint. In: 50th AIAA Aerospace Sciences Meeting Including the New Horizons Forum and Aerospace Exposition, p. 1187.
Yuan, W., Khalid, M., Windte, J., Scholz, U., Radespiel, R., 2005. An investigation of low-Reynolds-number flows past airfoils. In: 23rd AIAA Applied Aerodynamics Conference, p. 4607.
zçakmak, Ö.S., Sørensen, N.N., Madsen, H.A., Sørensen, J.N., 2019. Laminar-turbulent transition detection on airfoils by high-frequency microphone measurements. Wind Energy 22 (10), 1356–1370.
Zheng, X., Liu, C., Liu, F., Yang, C.I., 1998. Turbulent transition simulation using the k-ωmodel. Int. J. Numer. Methods Eng. 42 (5), 907–926.